Ripening of Ordered Breath Figures

Hartmut Gau

Max-Planck-Institut für Kolloid- und Grenzflächenforschung, Forschungscampus Golm, 14476 Golm, Germany

Stephan Herminghaus*

Abteilung Angewandte Physik, Universität Ulm, Albert-Einstein-Allee 11, 89069 Ulm, Germany
(Received 12 October 1999)

We have investigated the ripening of breath figures with variable initial order. A dramatic impact of the degree of order on the coalescence behavior is observed. As opposed to the two-droplet coalescence events common to the usual disordered droplet arrays, four-droplet coalescence cascades predominate in a perfectly hexagonal breath figure. Upon introduction of disorder, a gradual transition to a regime dominated by three-droplet cascades is observed. The statistics of coalescence cascades allows for detailed conclusions on the microscopic droplet dynamics.

PACS numbers: 68.45.Gd

When a liquid condenses from the gas phase onto a cold surface which is not wetted by the liquid, characteristic droplet patterns are generated which are called breath figures. The individual droplets are formed by heterogeneous nucleation on the substrate, and the resulting pattern is intrinsically disordered. Previous studies of breath figures have thus been restricted exclusively to disordered structures [1,2]. Emphasis was given to the investigation of statistical properties and scaling functions describing the droplet size distribution and its temporal evolution during the ripening process undergone via further adsorption of gas and coalescence of the droplets to larger ones [3–5].

The influence of a certain degree of order, which might be present initially in the droplet arrangement, has not been systematically studied to date. However, this is potentially of great importance, since at least partially ordered arrangements of droplets may form through processes such as spinodal dewetting [6–10], some order in the nucleation sites, or due to other structure formation processes in the adsorbate [11,12]. Furthermore, as it will become clear below, studying the ripening of ordered breath figures allows one to test certain assumptions widely used in their statistical description [13], which have not yet been examined experimentally.

We have generated hexagonally ordered aqueous breath figures by patterning the wettability of the substrate onto which the water was adsorbed. This was done by thermal evaporation of a polar compound (calcium chloride) through a suitable mask onto a hydrophobic substrate in high vacuum. As the substrate, we have chosen silicone rubber which was prepared by casting a precursor polymer ("Sylgard 184" purchased from Dow Corning) onto glass slides and then cross-linking thermally. This yielded very smooth surfaces (the roughness was ≈1 nm as revealed by scanning force microscopy) with an advancing contact angle of $108° \pm 2°$ with water. The receding angle was approximately $95°$, the hysteresis owing possibly to residual roughness, defects, chemical heterogeneity, and the softness of the substrate [14]. The mask has

been prepared by standard lithography and consisted of a 10 μm thick nickel sheet with a hexagonal arrangement of circular holes. The diameter of the holes was 5 μm, and the hole distance (primitive translation of the lattice) was 10 μm. Consequently, the calcium chloride deposit formed a regular lattice of circular patches on the sample which were thus rendered hydrophilic. The typical thickness of the patches was 0.4 nm ($\approx$1 ML), as determined with a quartz microbalance.

Upon cooling the sample by means of a Peltier element, water condensed on the hydrophilic patches, thus forming an almost perfect hexagonal lattice of droplets, as shown in the optical micrograph of Fig. 1. Just a few defects show up; their relative density was typically below 3×10^{-3}. No droplets are observed to nucleate and grow on the hydrophobic areas between the regular droplets. The total number of droplets on the sample (the figure shows a
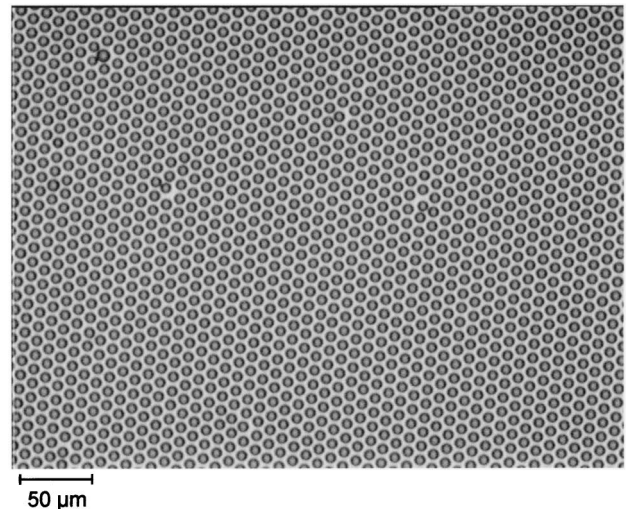
FIG. 1. A hexagonal breath figure, as formed by adsorption of water on a substrate with a hexagonal array of wettable patches. These consist of a soluble polar compound (calcium chloride) which finally dissolves in the droplets. When ripening sets in, the substrate is thus homogeneous again.

section only) is about 2100, adsorption rates were typically 30 nm/sec. Since the deposit is well soluble in water, each salt patch dissolves in the droplet forming upon it. Finally, an array of droplets of a dilute salt solution (≈ 10 mmol/l) on an unstructured substrate is obtained because all of the salt is dissolved. Thus, when the droplets grow further by condensation of water and coalescence finally sets in, the individual coalescence events will proceed without perturbation by a substrate structure, aside from the native substrate inhomogeneity. Since the salt content is small and changes only slightly during the coalescence scenario, the contact angle of the liquid on the silicon rubber substrate can be considered constant to a very high precision.

When the droplets in the hexagonal lattice have grown large enough to touch each other, the configuration will be as depicted in Fig. 2a, where each droplet "touches" six neighboring droplets. Let us contemplate the kind of coalescence events which are now expected to occur. Because of fluctuations, there will be one pair of neighbor droplets which touch and coalesce first. If the contact lines are sufficiently strongly pinned to defects on the substrate, we might expect that the larger droplet grows at the expense of the smaller one due to the difference in capillary pressure. As a consequence, this larger drop will "eat" all its six neighbors consecutively, being the largest of the ensemble of neighbors. The result is then a seven-droplet coalescence cascade, with the resulting large drop centered in a symmetric, hexagonal void.

On the contrary, if we neglect pinning completely and assume coalescence to be completely governed by inertia, the center of mass must be conserved, such that

$$\mathbf{x}' = \frac{m_1 \mathbf{x}_1 + m_2 \mathbf{x}_2}{m_1 + m_2} \tag{1}$$

for each individual two-droplet coalescence event, with $\mathbf{x}_1$, $\mathbf{x}_2$, and $\mathbf{x}'$ denoting the center of mass coordinates of the two initial droplets and the resulting droplet, respectively.

This has commonly been assumed to be fulfilled in most of the earlier work on breath figure ripening [13]. The result of Eq. (1) is illustrated in Fig. 2. Because of the geometric overlap after the first coalescence with the neighbor droplets, there will be a coalescence cascade combining finally four droplets to the configuration depicted in Fig. 2d. This is in marked contrast to the seven-droplet coalescence expected for strong pinning, as discussed above. Obviously, one should expect the coalescence process to depend sensitively on the detailed dynamics of the system.

In order to describe possible deviations from Eq. (1), we now introduce a parameter α by generalizing Eq. (1) to

$$\mathbf{x}' = \frac{m_1^{\alpha} \mathbf{x}_1 + m_2^{\alpha} \mathbf{x}_2}{m_1^{\alpha} + m_2^{\alpha}}. \tag{2}$$

For $\alpha = 1$, Eq. (1) is recovered, while $\alpha \to \infty$ represents strong pinning (i.e., the larger droplet rests in place). Using Eq. (2), we can perform a computer simulation of the
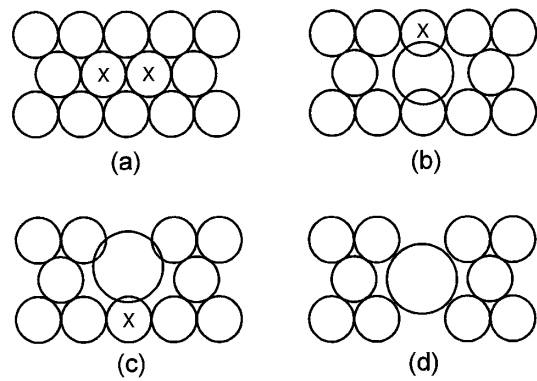
FIG. 2. (a) to (d): A model coalescence cascade at perfect hexagonal order, assuming conservation of the center of mass of the participating droplets, and of the total mass of the system. The droplets to coalesce next are marked with a cross in each sketch. Only after four droplets have coalesced, there will be no geometrical overlap anymore, and the cascade is expected to stop (d).

ripening of a perfect hexagonal droplet ensemble in the spirit of Fig. 2, but with variable α. Although it is not clear whether $\alpha < 1$ corresponds to a real physical system, we explored the whole range, $\alpha \in (0, \infty)$. As a result, we plotted in Fig. 3 the number n of droplets coalescing within one coalescence cascade, vs the parameter α. As expected, we obtain $n = 4$ for $\alpha = 1$, but there is in addition a lot of structure for $\alpha \neq 1$. In particular, we get runaway cascades, or avalanches, if α is below a critical value of 0.45 ± 0.02. For $\alpha \to \infty$, we do not obtain the simple result $n = 7$ derived above because fluctuations, which are absent in the simulation, are crucial for this type of cascade: Without fluctuations, the first coalescence of a cascade involves two droplets of exactly equal mass, such that according to Eq. (2), the resulting droplet will be situated half way in between them, even for $\alpha \to \infty$. In contrast, in a system with fluctuations, this will not happen because no two droplets will be *exactly* equally large.
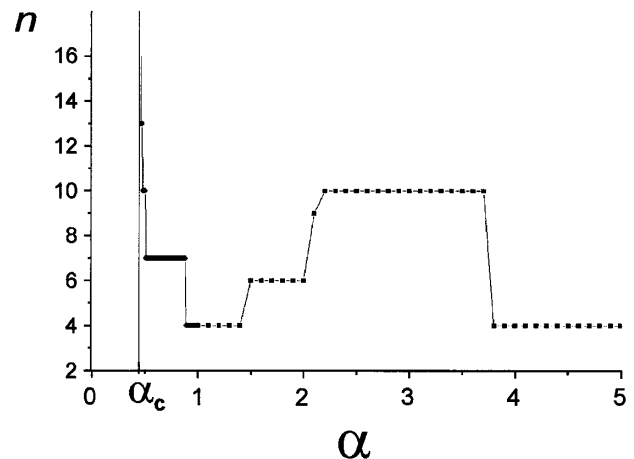
FIG. 3. The number of droplets n participating in a cascade, vs the parameter α defined in the text, as obtained from computer simulation.
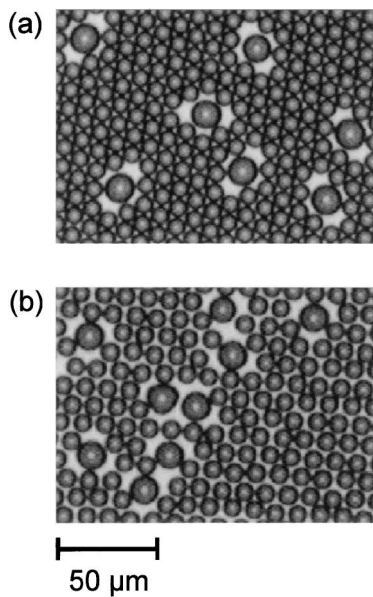
FIG. 4. (a) Typical ripening scenario observed experimentally for a perfect hexagonal lattice. Four-droplet cascades, such as depicted schematically in Fig. 2(d), predominate. (b) Same for a hexagonal lattice with some Gaussian disorder. Three-droplet cascades dominate, which resemble the structure sketched in Fig. 2(c).

Figure 4a shows a micrograph of the system presented in Fig. 1 after further adsorption, such that a number of coalescences has taken place. As one can see, the characteristic structures appearing are just as depicted schematically in Fig. 2d. This supports the model of cascades of consecutive two-droplet coalescence events as illustrated in Fig. 2. It further suggests, according to Fig. 3, that $0.9 < \alpha < 1.4$ in our system. It demonstrates experimentally the substantial impact of the degree of order of the initial droplet pattern on the coalescence dynamics, since the observed behavior strongly differs from the usual two-droplet coalescences as encountered very predominantly in the disordered case [13].

So far, our experiments have been restricted to perfectly ordered arrays. To introduce, a certain amount of disorder into the lattice in a controlled manner, we have heated the sample up to room temperature after it had already reached the state displayed in Fig. 1. As a consequence, the droplets evaporated again, while their centers of mass performed small scale random walks due to pinning of their contact lines to defects on the substrate surface. Finally, the salt concentration became high enough in each droplet for the salt to precipitate, and the dried state of the sample consisted of a lattice of salt patches the centers of which were slightly displaced from the perfect lattice sites. Upon cooling again (and consequent readsorption of water), a slightly disordered droplet lattice was obtained. Since the adsorption process is mainly governed by osmotic pressure, and each patch contained the same amount of salt, the droplet sizes were still equal. Thus, the disorder concerned the droplet positions only, not their sizes.

By repeating this procedure, the degree of disorder could be gradually increased. It could be quantified by the width w of the first peak of the two-point correlation function of the droplet centers. In what follows, w will be measured in units of the primitive translation of the lattice (10 μm, in our case). Since the random walks of the droplet centers during drying and readsorption can be assumed to proceed independently for each droplet, the disorder is expected to be well described by a 2D-Gaussian distribution of displacements relative to the perfect lattice sites. In fact, the peak in the correlation function could in all cases be well fitted by a Gaussian. The mere fact that we can introduce disorder in this way shows that pinning does play a role in our system, and the question is how strongly it affects the value of the parameter α.

Further adsorption leads to coalescence as above but, as Fig. 4b shows, with three-droplet coalescences now dominating, in place of the four-droplet coalescences in the perfect lattice. Within the time the orbit was taken, there were no cascades observed other than three-droplet and four-droplet. The process can be presented by plotting the total number of four-droplet cascades (N_4) which have happened during the adsorption process vs the total number of three-droplet cascades (N_3). The resulting orbit in the N_3-N_4 plane is shown in Fig. 5 for $w = 0.057$
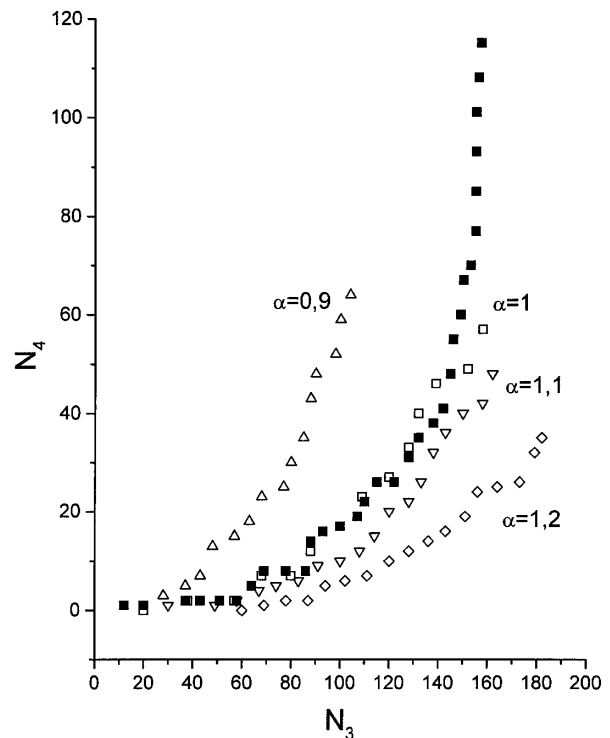
FIG. 5. Orbits N_4 vs N_3 (see text for definition). Full squares: experiment ($w = 0.057$). Open symbols: computer simulation for different α, but for the same disorder w (for perfect order, the orbit was found to be identical to the vertical axis, both experimentally and in the simulation). Within our accuracy, $\alpha = 1$.

as full squares. Although $w \ll 1$ is small, four-droplet cascades are almost completely suppressed in the beginning. The general observation is that in systems with small but nonzero w, ripening starts with three-droplet cascades alone, and four-droplet cascades take over later. The hexagonal order is lost when most of the initial droplets have coalesced, and the system approaches the usual scaling regime observed for disordered systems [5].

For comparison, the results of computer simulations for the same degree of Gaussian disorder, $w = 0.057$, but for different α are shown as open symbols. For $\alpha = 1$ (squares), the results agree perfectly (within scattering) with the experimental finding. This is in contrast to earlier attempts to describe the system in a mean field approach, which failed insofar as the parameter w had to be taken much larger than the experimental value in order to fit the orbits [15]. Since there were a few approximations made in the mean field approach, we acsribe its obvious failure to the high sensitivity of the system to details of the geometry. This is corroborated by the demonstrated dramatic impact of a small amount of disorder.

The simulation results for $\alpha = 0.9$ (upright triangles), $\alpha = 1.1$ (inverse triangles), and $\alpha = 1.2$ (diamonds) differ significantly from the experimental orbit. We thus have $\alpha = 1.00 \pm 0.03$ for our system, which means that the center of mass is quite accurately conserved during coalescence, in spite of the fact that there is noticeable pinning, which we have used for introducing disorder into the lattice. It should be noted that this accuracy in determining α would not be easily possible by microscopic inspection of individual cascades due to the limited resolution of optical microscopy. The method presented here of determining α works for all systems with droplets large enough for the symmetry of a coalescence cascade to be discernable, even if the individual droplets may be beyond the resolution of the microscope.

*Electronic address:
stephan.herminghaus@physik.uni-ulm.de

[1] D. Beysens and C. M. Knobler, Phys. Rev. Lett. **57**, 1433 (1986).

[2] B. J. Briscoe and K. P. Galvin, Phys. Rev. A **43**, 1906 (1991).

[3] F. Family and P. Meakin, Phys. Rev. A **40**, 3836 (1989).

[4] D. Fritter, C. M. Knobler, and D. A. Beysens, Phys. Rev. A **43**, 2858 (1991).

[5] P. Meakin, Rep. Prog. Phys. **55**, 157 (1992).

[6] J. Bischof, D. Scherer, S. Herminghaus, and P. Leiderer, Phys. Rev. Lett. **77**, 1536 (1996).

[7] S. Herminghaus *et al.,* Science **282**, 916 (1998).

[8] F. Vandenbrouck, M. P. Valignat, and A. M. Cazabat, Phys. Rev. Lett. **82**, 2693 (1999).

[9] R. Xie *et al.,* Phys. Rev. Lett. **81**, 1251 (1998).

[10] U. Thiele, M. Mertig, and W. Pompe, Phys. Rev. Lett. **80**, 2869 (1998).

[11] A. Mourran, S. S. Sheiko, and M. Möller, "Vitrified Condensation Pattern in Thin Polymer Films: A New Approach for Micropatterning" (to be published).

[12] L. V. Govor *et al.,* "Formation of Low Dimensional Structures on the Basis of Cellulose o-Nitrate" (to be published).

[13] D. Fritter, C. M. Knobler, D. Roux, and D. Beysens, J. Stat. Phys. **52**, 1447 (1988).

[14] C. W. Extrand and Y. Kumagi, J. Colloid Interface Sci. **184**, 191 (1996).

[15] H. Gau, W. Mönch, and S. Herminghaus, Progr. Colloid Polym. Sci. **110**, 34 (1998).